Using Rare-Earth Oxide Tracers for Studying Soil Erosion Dynamics

X. C. Zhang,* M. A. Nearing, V. O. Polyakov, and J. M. Friedrich

ABSTRACT

Spatially averaged soil erosion data provide little information on soil erosion dynamics. Dynamically varied, spatially distributed erosion data are needed to better understand erosion processes and thoroughly evaluate process-based erosion prediction models. The objectives of this study are to examine the feasibility of direct mixing rare-earth element (REE) oxides with soil materials to trace soil erosion at a plot scale and to explore further the potential of using this technique to study soil erosion dynamics. Five REE oxide powders were mixed with a Camden silt soil (fine, silty, mixed, mesic Typic Hapludalt) at five slope positions. Six rainstorms were applied to a 4 by 4 m soil bed at a 10% slope. Runoff was collected during the rains and surface soil was sampled after each rain. All samples were extracted for REE with a quick acid-leaching method and extracts were analyzed by inductively coupled plasma mass spectrometry (ICPMS). Mean error of REE-derived sediment discharge relative to measured total across six rainstorms was 14.5%. Our results demonstrate that the REE-tracing technique is feasible and sound, being capable of producing both spatially and temporally distributed erosion data. Results indicate that the most severe erosion occurred in the upper middle section of a uniform slope, and total sediment delivery from each segment was positively related to amounts of sediment deposition on the entire slope from that segment. This technique has the potential to bring new perspectives to soil erosion research.

Spatially averaged soil erosion data are useful for developing empirical erosion prediction models, understanding erosion principles, and deriving optimal erosion control management practices. However, such data are of limited value for understanding soil erosion dynamics such as temporal and spatial variations of soil detachment, sediment transport, deposition, and redetachment along a hillslope profile. Spatially and temporally distributed erosion data are needed not only to better understand soil erosion dynamics, but also for thorough validation of process-based erosion models. Spatially distributed soil erosion data are also useful for evaluating on-site impacts such as effects of soil redistribution on crop yields and off-site impacts including sediment origin and destination. Many process-based erosion prediction models have been developed in the past several decades to predict soil erosion at various temporal and spatial scales (Nearing et al., 1989; Hairsine and Rose, 1992; Borah, 1989). Since erosion processes constantly change in time and space, process-based models have advantages over spatially and temporally lumped empirical prediction models. However, these advantages will not be fully recognized unless the spatial and temporal predictability of process-based models are validated. Thus, spatially distributed erosion data are of great importance in advancing process-based erosion prediction models.

Various types of tracers have been developed and used to obtain spatially distributed data. Commonly used tracers include atomic bomb fallout radionuclide ^{137}Cs (Ritchie and McHenry, 1990; Walling and He, 1999), naturally occurring radionuclides ^{210}Pb, ^{7}Be, and ^{234}Th (Wallbrink and Murray, 1993), deliberately introduced radionuclides such as ^{56}Fe and ^{60}Co (Wooldridge, 1965; Toth and Alderfer, 1960), noble element (e.g., Au or Ag)-labeled natural particles (Olmez et al., 1994), REE-tagged particles (Riebe, 1995; Plante et al., 1999), and exotic materials including fluorescent dye-coated particles (Young and Holt, 1968), glass beads, and magnetic plastic beads (Ventura et al., 2001). Although these tracers have proven useful, each has limitations.

Bomb-produced ^{137}Cs (half-life of 30 yr) and naturally occurring ^{210}Pb (half-life of 20.2 yr) are widely used to estimate long-term soil erosion rates and erosion patterns across a landscape. However, these methods are quantitatively challenged by inconsistencies and uncertainties because of assumptions stemming from indeterminate input functions and indefinite spatial and depth distributions of the original deposition at the location of interest. For example, estimates of soil erosion rates associated with a particular level of ^{137}Cs depletion can vary by more than one order of magnitude when using calibration relationships derived under different assumptions (Walling and Quine, 1990). Above all, since uniform spatial distributions are always assumed, ^{137}Cs and ^{210}Pb provide little information on sediment origin.

Unlike bomb-produced and cosmogenic radionuclides, radioactive elements can be manipulated and deliberately introduced to study soil erosion. A major concern with this type of tracer is the radiological risk to researchers and the environment. Exotic particles such as fluorescent glass or magnetic plastic beads have been used to overcome this concern, but suffer other serious shortcomings. Major criticisms for exotic particles are that (i) these particles may not bind with soil particles or soil aggregates and therefore are transported separately; (ii) exotic particles differ in size distribution, particle density, shape, surface morphology, and surface chemical properties from soil particles and aggregates; and (iii) sensitivity of quantitative analysis is normally low, which means that a large quantity of tracers are needed to trace soil and sediment movement on a hill slope or in a small watershed.

X.-C. (John) Zhang, USDA-ARS, Grazinglands Research Lab., 7207 W. Cheyenne St., El Reno, OK 73036; M.A. Nearing and V. Polyakov, USDA-ARS, National Soil Erosion Research Lab., Purdue Univ., West Lafayette, IN 47907; and J.M. Friedrich, Dep. of Chemistry, Purdue Univ., West Lafayette, IN 47907. Received 6 Nov. 2001. *Corresponding author (jzhang@grl.ars.usda.gov).

Published in Soil Sci. Soc. Am. J. 67:279–288 (2003).

Abbreviations: REE, rare-earth element; DEM, digital elevation map; ICPMS, inductively coupled plasma mass spectrometry.

Labeling natural sand particles with noble metals (e.g., Au, Ag) or glass particles or ceramic prills with REE circumvents most drawbacks discussed above. These elements can be analyzed by neutron activation analysis. However, it is extremely difficult to produce such labeled particles that resemble the size distribution, particle density, shape, surface morphology, and surface reactivity of the ambient soil. Besides, labeling procedures can be tedious and time-consuming if a large quantity of tracer is required.

Tracers ideal for studying soil erosion and sediment dynamics should overcome the above drawbacks and possess the following properties: strong binding to soil particles or ready incorporation into soil aggregates, high analytical sensitivity, easy and inexpensive to quantify, low background soil concentration, no interference with sediment transport, low plant uptake, be environmentally benign, and be available in variants with similar physicochemical properties but distinct in signature for unbiased tracing of multiple sediment sources.

The Lanthanide series elements, or REE, possess all of the preceding properties of ideal tracers. Zhang et al. (2001) reported that REE oxide powders, when directly mixed with a silt loam soil, were uniformly incorporated into soil aggregates of different sizes and were bound with silt fractions. They also developed and tested a quick acid-leaching method for extracting REEs from soil and sediment samples for analysis by ICPMS. The quick extraction method makes it possible to take full advantage of this new technology. The advantages of ICPMS as identified by Jarvis (1989) include exceptional detection limits for all REEs (in the range of nanograms per kilogram [ng kg^{-1}] to micrograms per kilogram [μg kg^{-1}]), uniform sensitivity across the mass range, multiple element capability, rapid analysis time (minutes per sample), and no need for chemical separation.

A few experimental studies have been conducted to monitor soil erosion using REE oxides. Riebe (1995) used europium-labeled glass particles to trace soil translocation. During manufacturing, Plante et al. (1999) tagged ceramic prills with dysprosium oxide to study soil aggregation and translocation. Directly labeling the particles with REE oxides was done to ensure that the dysprosium and particles were bound together. Zhang et al. (2001) demonstrated that REE oxides, when directly mixed with soil, were bound with fine soil particles and incorporated into soil aggregates in uniform proportions. This finding has shown that there is no advantage in tagging exotic particles with REEs for soil erosion studies. Tian et al. (1994) and coworkers (Institute of Soil and Water Conservation, 1997) conducted a few pioneering experiments by directly mixing REE oxides with soils at different slope positions to monitor soil erosion. They reported that their results were satisfactory and the tracing method was promising.

The objectives of this study are to examine the feasibility of directly mixing REE oxides with soil materials for tracing soil erosion on a 4 by 4 m plot and to explore the potential of using this technique for studying soil erosion dynamics.

MATERIALS AND METHODS

Soil Characteristics

The Ap horizon of a Camden silt soil (mixed, mesic Typic Hapludalt) was sampled near West Lafayette, IN, and passed through an 8-mm sieve at around 10 to 15% moisture. The Camden silt soil was approximately 8% clay and 87% silt. The background concentrations of Gd, Sm, Pr, La, and Nd elements in this soil were 2.98, 3.18, 4.38, 17.06, and 16.29 $\mu g\ g^{-1}$, respectively.

Rare-Earth Oxide Characteristics

Five REE oxides (La_2O_3, Pr_6O_{11}, Nd_2O_3, Sm_2O_3, and Gd_2O_3), selected on the basis of cost, were imported from the People's Republic of China. Selected physical and chemical properties of REE oxides are given in Table 1. Purity and REE oxide content were determined with ICPMS (Zhang et al., 2001). Particle-size distribution of REE oxide powder was measured by a pipette method and D50 was computed from the measured distribution (Zhang et al., 2001). The particle density was obtained from the manufacturer.

Soil Bed Preparation and Rare-Earth Element Application

A wooden box (4 by 4 m) with adjustable slope was used in the study. The box was arbitrarily set to a 10% slope, partially because it is close to the standard 9% slope used for developing the Universal Soil Loss Equation. The sieved soil was packed into the soil box to a depth of 0.2 m over a 0.5-m sand layer, which drained freely. The bulk density of the packed soil was approximately 1.3 Mg m^{-3}. The soil surface was gently packed to remove microrelief with a wood block. The soil bed was prewetted and kept wet between rains with trickle irrigation tubes placed on the upper slope segment at a rate without incurring surface runoff.

The soil box was divided into five equal segments of 0.8 m each (Fig. 1). A 0.15-m band, located two thirds of the way down each imaginary segment, was tagged with a randomly selected REE oxide to represent the average soil erosion rate of that segment. Approximately 19% of the area in each segment was tagged with tracers. The purposes for choosing the band application strategy are to explore an easy application method for field use and to assess erosion estimation error associated with partial area tagging. Tracing depth, based on potential erosion rates, was 30 mm for the Gd, Sm, and

Table 1. Selected physical and chemical properties of the five rare-earth element (REE) oxide powders.

Chemical formula	REE oxide	Purity†	D_{50}‡	Particle density
	%		μm	Mg m^{-3}
Gd_2O_3	96.54	98.97	2.19	7.41
Sm_2O_3	95.91	98.14	3.61	7.68
Pr_6O_{11}	91.86	95.53	16.38	6.83
La_2O_3	80.09	98.44	1.23	6.51
Nd_2O_3	84.63	99.02	3.65	7.24

† REE oxide of interest divided by total of the five REE oxides
‡ A particle size at which 50% of sample mass is greater than that size.

Nd bands and 50 mm for the Pr and La bands. The tracing depth will not affect experimental results as long as soil erosion, especially rilling, does not occur below the tracing depth. The shallower tracing depth is merely to reduce tracer use. Soil was removed from each band to the designated depth, and total soil mass was measured. To facilitate REE-soil binding, the excavated soil was moistened to 15 to 20% water content. The moistened soil was then mixed with a predetermined amount of REE oxide in a dilute fashion to ensure uniform mixing. After thorough mixing, the mix was back-filled to the excavated volume. Care was taken to ensure there was no cross contamination between segments. Doped REE concentrations in each band and representative concentrations for each segment are given in Table 2.

Soil Surface Elevation Scanning

A 4 by 4 m laser scanner (Huang and Bradford, 1990; Flanagan et al., 1995) was used to obtain a digital elevation map (DEM) of the soil surface after each rainfall.

Scanning resolution was set to 6 by 6 mm in the horizontal directions, and 0.2 mm in the vertical direction with a standard deviation of 0.13 mm on a smooth surface. Four aluminum pins were installed at each corner of the plot to ensure no movement of the scanner frame between rains and to provide a reference elevation for the DEM. Arc-View GIS software was used to convert raw scan measurements to relative elevation data using a calibrated second-order polynomial equation. Resultant DEMs were used to calculate net volume changes of each rain by subtracting the two surfaces before and after each rain. The volume was then converted to soil mass using a mean bulk density of 1.3 Mg m^{-3}.

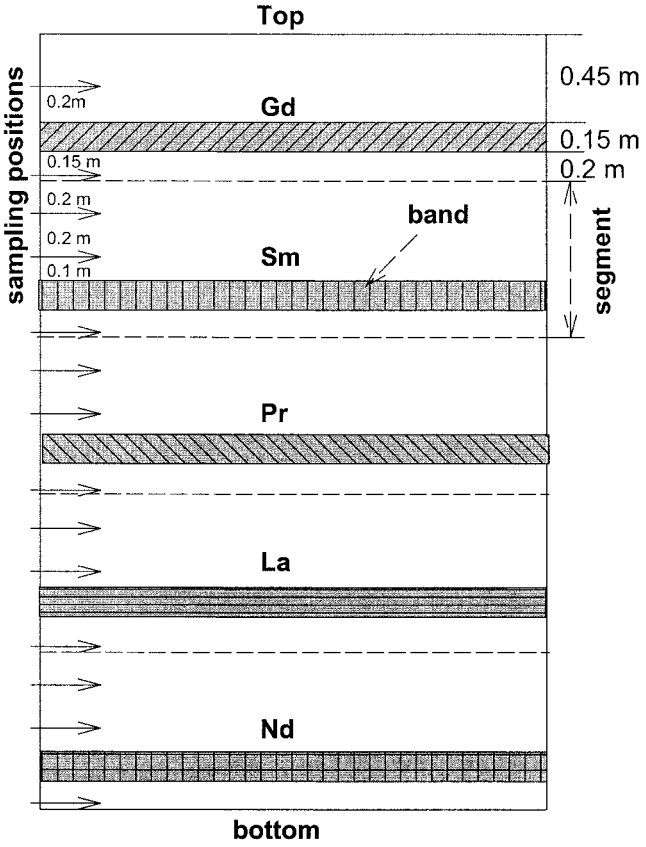

Fig. 1. Schematic representation of experiment setup.

Rainfall Simulation and Sediment Sampling

Four rainfall simulators with oscillating type nozzles were placed in parallel across the slope. A standard nozzle spacing of 1.15 m was used, and the measured spatial coefficient of variation of rainfall intensity was <7.5%. Six consecutive rain events were applied to the soil bed at roughly 3-d intervals. All rains lasted 1 h. The target rainfall intensity was 60 mm h^{-1} for the first four rains and 90 mm h^{-1} for the last two. Runoff and sediment were collected at the lower end of the bed at 2-min intervals, and measured gravimetrically. After oven drying, every three consecutive samples were combined, crushed to <2 mm, and mixed well for REE extraction. Each combined sample represents a 6-min period.

Surface Soil Sampling

Open-ended rectangular boxes (30 by 20 by 10 mm), made of aluminum sheets, were used to take soil samples. The box, laid across the slope, was gently pushed into the soil until the top edge lined up with the soil surface. The sample was dug out and trimmed with a knife to ensure a 10-mm sampling depth. The sample hole was then back filled with the same blank soil to minimize surface disturbance. Two samples, taken at the same slope length and about 0.2 m apart, were combined to form a composite sample to represent that slope length position. Fourteen composite samples were taken after each rain along a longitudinal transect at 14 slope length positions (Fig. 1). Two samples (one at 0.2 m above the upper tracing band and the other at 0.15 m below) were taken for the upper most Gd segment. Three samples (two at 0.3 and 0.1 m above the tracing band and one at 0.15 m below) were taken for each of the remaining segments. Only one sample was taken above the Gd tracing band because there was no upslope sediment delivery into the segment and REE concentrations were close to the background values near the top border. The transect was right-shifted (facing the bed) about 0.3 m after each rain. All samples were air-dried and crushed to <2 mm.

Rare-Earth Element Extraction

A simple, quick acid-leaching procedure, similar to that used by Zhang et al. (2001), was used to extract REEs from all soil and sediment samples. The procedure follows: (i) weigh 2 g of soil sample into a 50-mL Erlenmeyer flask; (ii) add 10-mL concentrated HNO_3 (70%, w/w), and reflux at 85°C in a water bath for 2 h; (iii) after cooling to <70°C, add 10 mL of H_2O_2 (30%, w/w) slowly to remove organically bound REEs, and heat the solution for 2 to 3 min after effervescence subsides; (iv) add 5 mL of concentrated HCl (36%, w/w) and reflux at 85°C in water bath for 2 h; (v) filter with

Table 2. Doped rare-earth element (REE) concentration in each band, representative REE concentration in each segment, soil background concentration, and extraction efficiency of each element.

Element or Segment	REE concentration in			Extraction efficiency
	Tracing band	Segment	Background	
	μg g^{-1}			%
Gd	5767.5	1081.4	2.98	93.51
Sm	5697.5	1068.3	3.18	87.76
Pr	5613.2	1052.5	4.38	87.72
La	5052.3	947.3	17.06	97.97
Nd	5543.2	1039.4	16.29	110.57

No.5 Whatman (Whatman Ltd., Clifton, NJ) filter paper 24 h into the extraction, and elute with 5 mL of deionized water (18 MΩ cm^{-1}); (vi) filter through a 0.45-μm membrane.

Two replicates were made for each sample and the mean was used in all analyses. Extraction efficiency, defined as the percentage of added REE that was recovered by the extracting procedure, is given in Table 2 for each REE. A value of >100% for Nd might have resulted from nonuniform mixing of doped soil samples.

Inductively Coupled Plasma Mass Spectometry Sample and Standard Preparations

A 100-mg aliquot of each extract was transferred to a 50-mL polyethylene centrifuge tube and massed exactly. Stock internal standard solution containing In and Tl was added to the tube, massed, and the volume was brought to 50 mL with 18 MΩ cm^{-1} water. Final internal standard concentration was approximately 10 ng g^{-1} for all samples and standards. Total acid concentration of final analyzed solution was 1 to 1.5%.

External calibration standards were prepared from a certified stock REE solution (SPEX Sample Preparation, Metuchen, NJ; 10 μg g^{-1}) by serial dilutions in concentrations of 0, 5, 25, 60 ng g^{-1}. Calibration standards were matched in acid concentration (1.5%) and composition (HCl and HNO_3) to a typical sample. Using these standards, all sample concentrations fell within the calibration range. Three replicates of each dilution were prepared for each sample and each dilution sample was analyzed once, using ICPMS.

Inductive Coupled Plasma Mass Spectrometry Data Correction

Raw, integrated counts per second data were processed in three sequential steps by an in-house computer program. First, the program normalized differences in internal standard concentrations between individual samples and standards. A linear scaling was used to normalize internal standard concentration of standards, samples, and blanks. Second, correction for intersample instrument response was done by linear interpolation between the two internal standards based on mass (adjustment for mass-dependent drift). Third, blank counts were subtracted from sample and standard counts, and these modified standard counts were used to compute a linear calibration of response versus concentration. From this equation, concentrations in soil sample aliquots were calculated. Finally, dilutions and soil sample masses were accounted for to yield the REE concentration in the soil.

Sediment Rare-Earth Element Data Analysis

Sediment REE concentration directly measured by ICPMS needs to be corrected for soil background concentration and extraction efficiency of the REE in question (Table 2). The corrected concentration of sediment from segment or tracer i in Time Step j (CC_i^j) can be computed as

$$CC_i^j = (C_i^j - B_i)/E_i \quad [1]$$

where i is the tracer or segment index, j is the time-step index, C is the ICP-measured REE concentration, B_i is the background concentration of tracer i, and E_i is the extraction efficiency for tracer i.

The amount of sediment that originated in a given segment i and was delivered to the outlet of the plot during Time Step j, L_i^j, can be estimated from mass balance considerations as

$$L_i^j = T^j \times CC_i^j/O_i \quad [2]$$

where T^j is the total sediment mass collected as sediment discharge during time j, and O_i is the original average concentration of the tracer for segment i (Column 3 in Table 2). Equation [2] can be rearranged into

$$L_i^j/T^j = CC_i^j/O_i = R_i^j \quad [3]$$

where R_i^j is defined as the sediment ratio (ratio of sediment discharge that originated from segment i to that measured total during Time Step j). The sediment ratio based on Eq. [3] is equal to the concentration ratio (ratio of concentration of tracer i in sediment collected during Time Step j to that original average concentration), which can be easily estimated with measured concentrations. The total REE-estimated sediment ratio for Time Step j is then the sum of R_i^j for all i as

$$R^j = \Sigma\, R_i^j \quad [4]$$

The R^j should be equal to 1 if the REE method is accurate. A value of $R^j > 1$ indicates an overprediction of total sediment yield for Time Step j, while <1 yields an underprediction. Likewise, the overall estimation ratio, R, for the entire rainfall is the sum of R^j for all j

$$R = \Sigma\, w^j R^j \quad [5]$$

where w^j is the weighting factor for Time Step j based on the proportion of total sediment generated during Time Step j.

Soil Rare-Earth Element Data Analysis

Rare-earth element concentrations in the surface soil samples also need to be corrected for the background concentrations and extraction efficiencies. Again based on mass balance, deposition at position k (sampling locations) from segment i after rain n (D_{ik}^n) can be computed as

$$D_{i\,k}^n = CC_{i\,k}^n \times M_k/O_i \quad [6]$$

where M_k is the sample mass from position k. Total deposition at position k from all segments above after rain n (D_k^n) is the sum of D_{ik}^n for each segment i. If we assume that D_k^n is representative of the average deposition rate in the area between positions k and $k + 1$, the overall total deposition along the entire slope profile after rain n (D^n) is

$$D^n = \Sigma\ (D_k^n \times A_k) \text{ for all } k \qquad [7]$$

where A_k is the area between positions k and $k + 1$. Note total deposition is an effect of cumulative deposition that occurred from the beginning of the first rain to the end of the rain in question. Thus, net deposition per rain is equal to $D^n - D^{n-1}$, where $n - 1$ is the number of the previous rain.

If we assume that deposition from previous rains will be retranslocated by erosion including splashing in each subsequent rain, sediment delivery ratio for rain n (ρ^n) may be estimated by

$$\rho^n = Y^n/(Y^n + D^n) \qquad [8]$$

where Y^n is the measured total sediment discharge for rain n. The sediment delivery ratio for a rain event is defined as the ratio of sediment discharge at the outlet to the sum of sediment discharge plus deposition on the slope during that event. Thus, the delivery ratio estimated with Eq. [8] is exact only for the first rain because D^n is cumulative. For subsequent rains, Eq. [8] gives lower-bound estimates because deposition from previous rains may not be entirely retranslocated as assumed. Based on changes in net deposition during a rainfall event, an erosion equilibrium index (κ) for that event can be defined as

$$\kappa^n = Y^n/(Y^n + D^n - D^{n-1}) \qquad [9]$$

κ should equal 1 when the whole erosion system that consists of detachment, transport, and deposition is in equilibrium. The equilibrium means that neither net deposition nor net detachment occurred during the event. That is, both net deposition and net detachment are zero. Thus, κ would be <1 when net deposition predominates and >1 when net detachment prevails.

RESULTS AND DISCUSSION

Runoff and sediment discharges for the six consecutive rains are plotted with time in Fig. 2. Runoff corresponded well with rainfall intensity except for Rain 1. Runoff during the first rain only began after 15 min because of the freshly packed, unsealed soil surfaces that infiltrated water easily at the beginning of the experiment (Fig. 2A). Runoff discharge gradually approached steady state after 45 min. In contrast, runoff discharge reached steady state within a few minutes in all the subsequent rains, resulting from a fully developed surface seal. Initial soil moisture contents of all events were similar and close to saturation as wetted by dripping tubes. Sediment discharge followed a trend similar to that of surface runoff (Fig. 2B). The three distinct runoff and sediment discharge scenarios provide an opportunity to study the relative dominance of erosion versus deposition under the different runoff and sediment regimes.

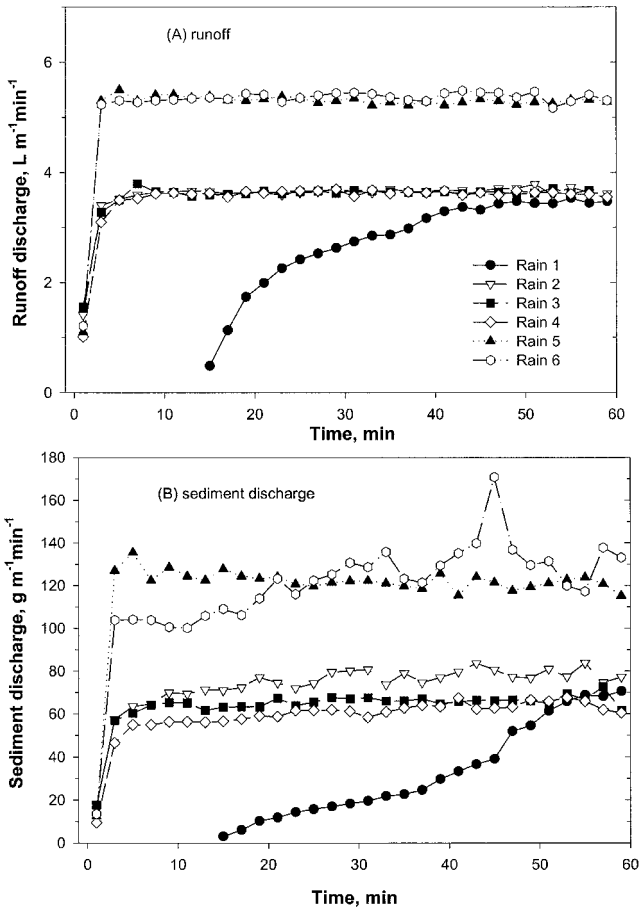

Fig. 2. Plot of (A) runoff and (B) sediment discharges vs. time for six rainfall events.

The REE-derived sediment discharges, calculated as the summation of L_i^j in Eq. [2] for all i and j, reflect how application of REE concentration ratios modified sediment discharge measurements. These estimates agreed reasonably well with those of measured totals for all six rains (Fig. 3). The goodness of estimation was more directly shown by the overall estimated sediment ratio, R of Eq. [5]. Ratio R is actually a quotient of sediment discharge of REE-derived event total to that of measured total, and therefore a good measure of the accuracy and validity of the method. On a percentage basis, the method overestimated sediment discharge by 26, 25, 17, 8, 7, and 4% for Rains 1 through 6, respectively (Table 3), showing a steady increase in accuracy with each subsequent rain. Overestimation, especially seen in the first three rains, may have resulted from the band tracing method, in which only 19% of the segment area was tagged with tracers. Because of the spatially variable nature of soil erosion, the band-tracing method, though easier to apply in the field, may be less accurate than applications where 100% of the surface area is tagged. Since measured sediment discharge is spatially lumped, total erosion estimates should be more accurate with a larger tagged fraction. During subsequent rains, the literally untagged areas will be variably covered by

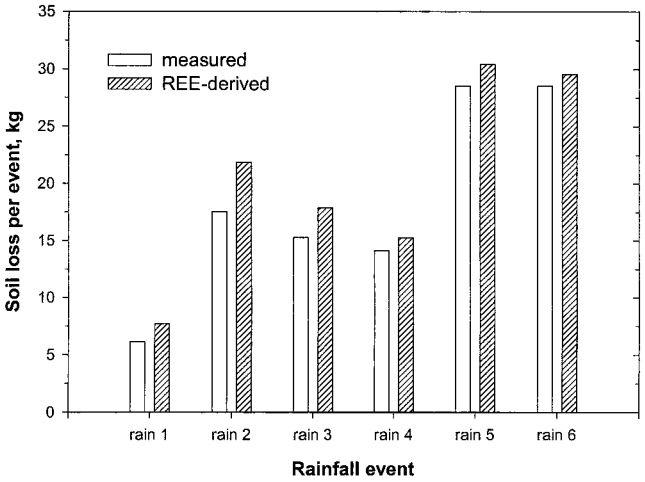

Fig. 3. Histogram of measured and rare-earth element (REE)-derived total sediment discharge per rain for six rainfall events.

tagged soil materials because of sediment deposition (as indicated by REE concentration distribution in surface soil below). As a result, overall event-averaged accuracy was improved throughout subsequent rains. This suggests a whole area-tracing method may give greater accuracy. However, considering that the relative difference of measured soil loss between replicated field plots can be as high as 200% (Nearing et al., 1999), relative errors of <30% might be acceptable and worth the sacrifice for the ease of tracer application.

Rare-earth elements estimated sediment ratios for Time Step j, R^j (Eq. [4]), were relatively stable and close to 1 throughout each individual rain except for Rain 1 (Table 3), in which R^j decreased rapidly with time, showing a decreasing impact of the initial tracing conditions. The abnormally high sediment ratios in the first two periods of Rain 1 might mean that the partial area tracing method (band application strategy) assumption that soil erosion rates from each band area represent the average erosion rates of that segment was not completely valid. Because of spatial variability of soil erosion, the band-tracing method could either over or underestimate sediment discharge from each segment, depending on the location of severely eroded spots. For example, development of a scouring hole near the La band area led to considerable overestimation of sediment discharge from that segment. However, the stable and near unity R^j values for each time interval during the subsequent rains demonstrate the capability of this tracing technique for studying transient sediment delivery and sources.

Table 3. Sediment ratio in each time period (R^j) and for the entire event (R) of six consecutive rainfall events.

Period	Rain 1	Rain 2	Rain 3	Rain 4	Rain 5	Rain 6
min						
0–6		1.20	1.16	1.06	0.94	1.06
6–12		1.25	1.09	0.98	0.91	1.07
12–18	1.97	1.27	1.13	1.00	1.02	1.12
18–24	1.87	1.30	1.22	1.04	1.14	0.99
24–30	1.36	1.31	1.16	1.08	0.91	1.01
30–36	1.43	1.29	1.20	1.09	1.18	0.91
36–42	1.27	1.25	1.22	1.07	1.14	0.84
42–48	1.09	1.22	1.20	1.20	1.16	0.99
48–54	1.19	1.21	1.17	1.12	1.12	1.18
54–60	1.20	1.17	1.16	1.14	1.12	1.23
Overall event (R)	1.26	1.25	1.17	1.08	1.07	1.04

The dynamic, REE-estimated sediment delivery from each segment (calculated with Eq. [2]) is shown with time in Fig. 4 for Rains 1 and 3 as an example. During Rain 1 (Fig. 4A), except for the La segment, each segment's REE sediment discharge increased with time as surface runoff increased (Fig. 2). The sediment discharges from the Sm and Pr segments increased more quickly than the others. This may indicate that the Sm and Pr segments (upper middle section) were predominated by detachment and the La and Nd segments (lower section) by transport, with the upper most Gd segment being limited by transport because of low surface runoff. The initial large sediment discharge from the La segment was partially because runoff initiated in the lower section and a scouring hole was developed near the La band area. Because of sediment deposition near the end plate, which caused a change in slope, net detachment from the Nd segment was limited.

The proportions of sediment discharges from the top two segments (i.e., Gd and Sm), compared with the other segments, were somewhat larger in Rain 3 than in Rain 1 (Fig. 4B). It is believed that redetachment of

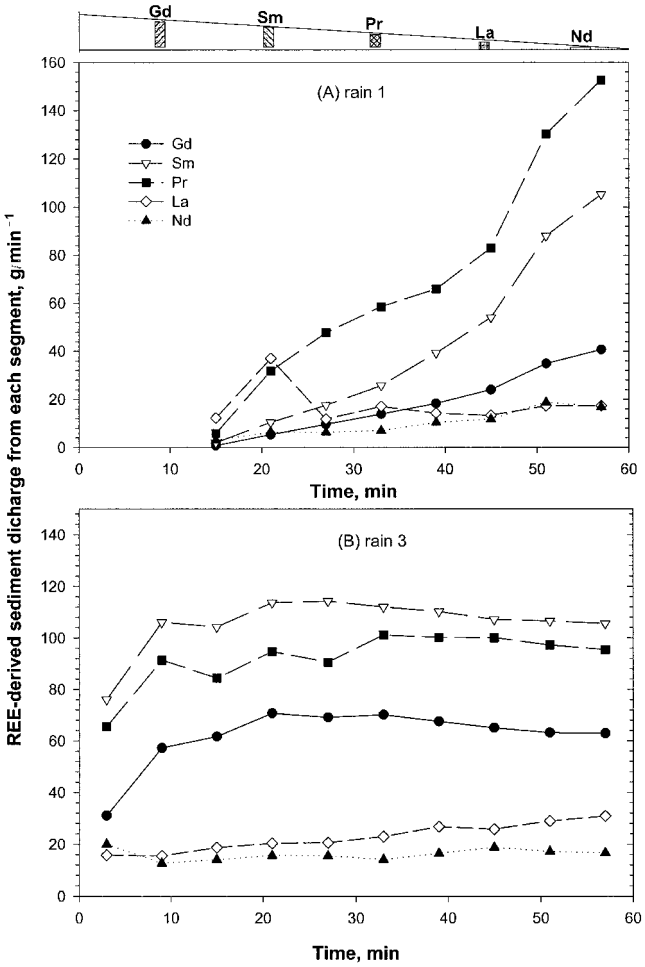

Fig. 4. Rare-earth element (REE)-derived sediment discharge from each traced-segment during (A) Rain 1 and (B) Rain 3.

previously deposited sediment along the slope surfaces was responsible for the increase. However, since very little net detachment occurred during the third rain (see data below), a quasi-steady state of sediment delivery was considered to have existed in Rain 3. At the steady-state condition, more sediment was delivered from the upper middle section than the lower section (Fig. 4B). This result supports the sediment feedback concept (Foster and Meyer, 1972), which states that sediment detachment rates are inversely related with sediment loads. That is, the upper middle section (where sediment load was low) was predominated by detachment, whereas the lower section was controlled by transport because of high sediment load from upslope and the reduced slope gradient stemming from sediment deposition near the end plate.

Data from each segment for the six rains, which were estimated with both the REE and laser-DEM methods, are presented in Fig. 5. The DEM method measured the net volume change of each segment and provides no indication of where the eroded sediment may have ended up; whereas, the REE method reflected the original source of sediment that was delivered to the outlet, some of which may have been redetached from the earlier deposits as a secondary source. Theoretically, the two methods measure two different entities; however, under steady-state sediment delivery conditions, the difference between the two entities diminishes. Interestingly, both methods revealed a similar spatial pattern of soil erosion, which may indicate that sediment delivery was at or near steady state for much of the time.

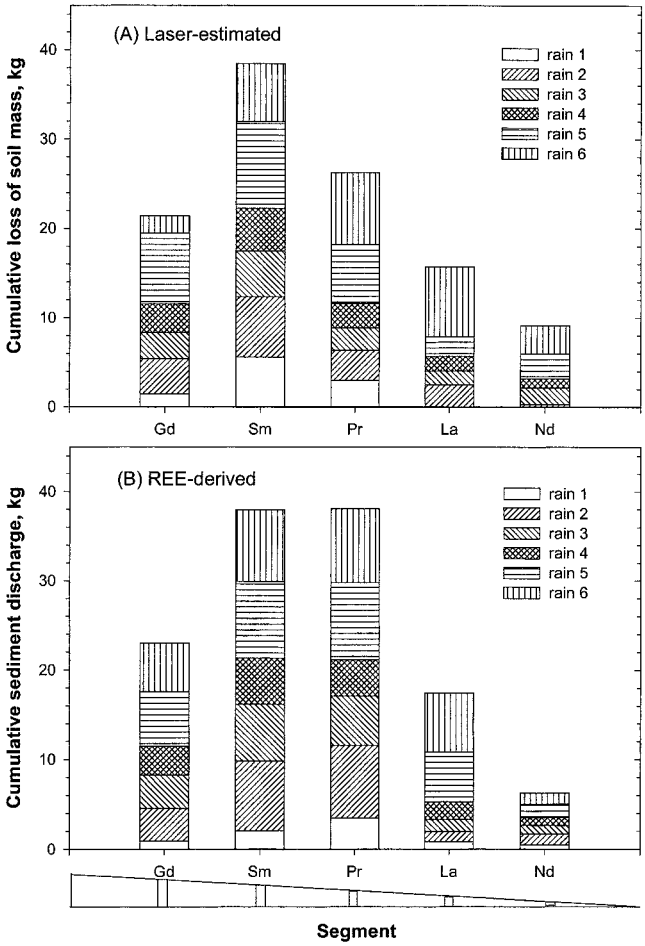

Fig. 5. (A) Laser-measured and (B) rare-earth element (REE)-derived cumulative sediment discharge from each traced-segment for six consecutive rainfall events.

Both methods revealed that the most severe net soil erosion occurred in the Sm and Pr segments (Fig. 5). The large difference between the two methods for the Pr segment resulted from deposition in the interrill areas and severe erosion in the rill areas. The interrill deposition reduced the scanned net volume change and therefore the net removal of soil mass, while the severe rilling provided an ample sediment discharge from the segment. Both methods show that the sediment discharge from the Nd segment was the least, and the sediment discharge from the La segment was less than that from the Gd segment. These results suggest that a transport-limited process regime existed in the lower plot section, especially in the Nd segment. In the La segment, the transport process predominated during the first four rains in which rainfall intensity was 60 mm h^{-1}. The detachment process was intensified during Rains 5 and 6 when rainfall intensity was increased to 90 mm h^{-1}. The increased runoff discharge or stream power was not only able to transport greater sediment loads from the upper slope segments but also detach additional soil or sediment from the La segment. The overall results obtained from this experimental study contradict the wisdom that severe erosion occurs in the lower section on a uniform slope. However, these preliminary findings need to be further tested at longer slope lengths and at various slopes to examine the end plate effect.

Rare-earth element concentrations in the surface soil layer sampled after Rains 1, 3, and 5 are presented in Fig. 6. The selection of the alternating rain events is merely to improve the graph readability. Rare-earth element concentrations in the surface soil samples are dependent on sampling depth because of deposition. Deposition depth was assumed to be <10 mm and therefore the 10-mm sampling depth was used. Since the same sampling depth was used throughout, relative comparisons of REE concentrations between tracers were deemed valid. However, because of a shift of sampling locations following each rain, strict comparisons between rains should be considered with some caution. There was a general trend that REE concentration of each tracer decreased rapidly with distance down slope of each tracing band. There was consistent sediment deposition from all segments in the immediate upslope of the end plate. The Gd concentrations on the slope profile tended to increase from Rain 1 to Rain 3 to Rain 5 because of cumulative deposition. Lack of consistent trends above the end plate deposition area for other tracers reflects the highly variable nature of erosion processes (i.e., simultaneous and interactive detachment, transport, and deposition) both in space and time.

Amounts of deposition at each sampling location k (D_k^n) following Rains 1, 2, and 3, estimated by summing Eq. [6] for all segment i above the location, are plotted with down slope distance in Fig. 7. In essence, D_k^n re-

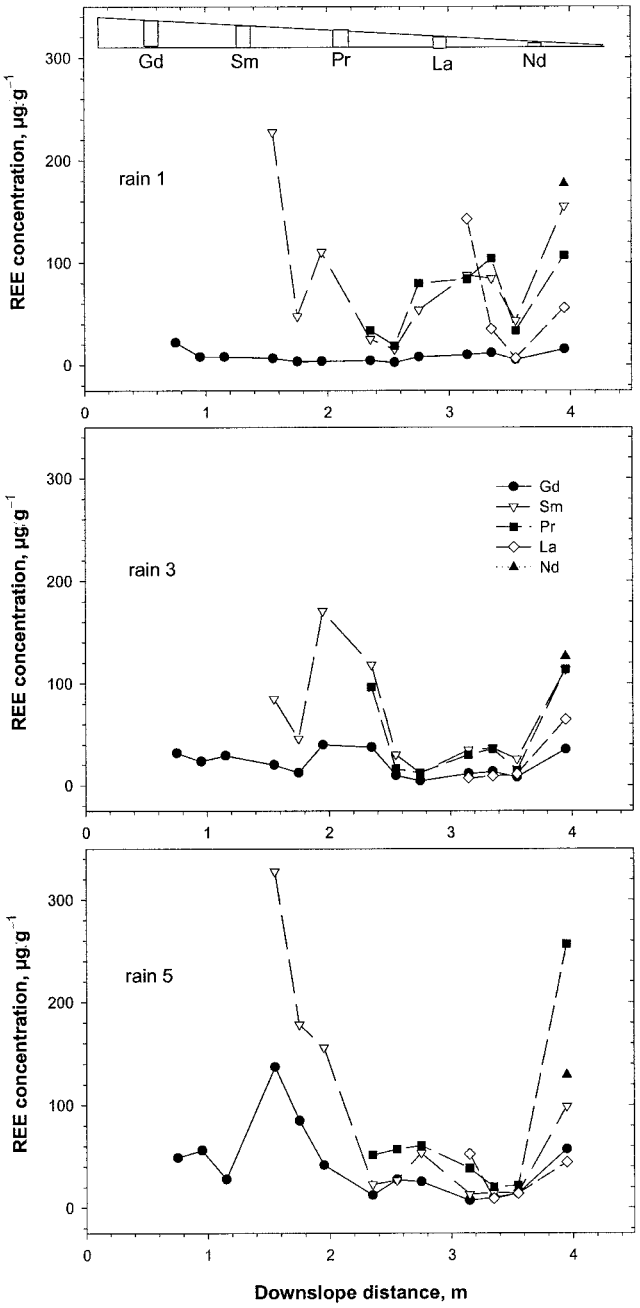

Fig. 6. Longitudinal distribution of rare-earth element (REE) concentration in the 10-mm surface soil layer following Rains 1, 3, and 5.

flected a cumulative effect of deposition that occurred from the beginning of the first rain to the end of any given rain. The results indicate that sediment deposition varied considerably down the slope profile. There were relatively high deposition zones between 1.2 and 2.4 m in the Sm and Pr segments and below 3.6 m in the Nd segment. Surprisingly, Fig. 5B shows that the most severe erosion also occurred in the Sm and Pr segments during these three rains. These seemingly contradictory results suggest that detachment and transport processes occurred simultaneously and interactively during each erosive rain, and could be better understood by the interrill-rill erosion concept. That is, severe erosion took

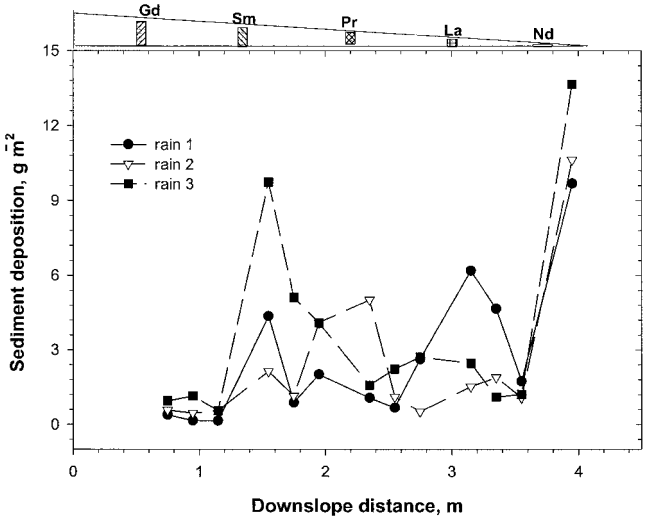

Fig. 7. Total (cumulative) deposition at each sampling location following Rains 1, 2, and 3 (D_k^n, expressed on a unit area basis).

place in the rill areas while transient sediment deposition occurred in the interrill areas. This result agrees with the explanation given earlier regarding the large discrepancy between the REE-derived and laser-estimated erosion in Fig. 5. Large amounts of deposition in the Nd segment were results of the lower plot boundary effect.

Total sediment deposition on the entire slope profile following each subsequent rain (D^n), calculated with Eq. [7], is shown in Fig. 8 for all six rains. Total deposition amounts following each rain were results of the continuous deposition that occurred from the first rain to the end of any given rain. Therefore the net deposition or net detachment occurring during a single rain would be the difference of the two adjacent bars (i.e., $D^n - D^{n-1}$). A positive value signifies net deposition while a negative value represents net detachment. Net deposition or gain occurred only during the first and fifth rains, while small net detachment occurred during the subsequent rains. Obviously, substantial net deposition occurred in Rains 1 and 5 when rainfall intensity was jumped from 0 to 60 mm h^{-1} for Rain 1 and from 60 to 90 mm h^{-1} for Rain 5. This may be because the interrill erosion that is determined largely by rainfall intensity (Zhang et al., 1998) is increased instantaneously as rainfall intensity is increased while the rill erosion that depends on rill flow hydraulics is increased slowly as a flow network or flow depth distribution is gradually developing or adjusting. This is especially true for Rain 1 as surface runoff was low and increased slowly with time. In contrast with Rains 1 and 5, small amounts of net detachment occurred in Rains 2, 3, 4, and 6, indicating that more efficient sediment delivery networks were being formed. However, the amounts of net detachment were 12, 12, 21, and 5% of total sediment discharges collected at the plot outlet for Rains 2, 3, 4, and 6, respectively. The small net detachment may indicate that quasi-steady state detachment and transport systems may have been formed in these rains following the disturbance of the previous equilibrium because of changes in rainfall intensity.

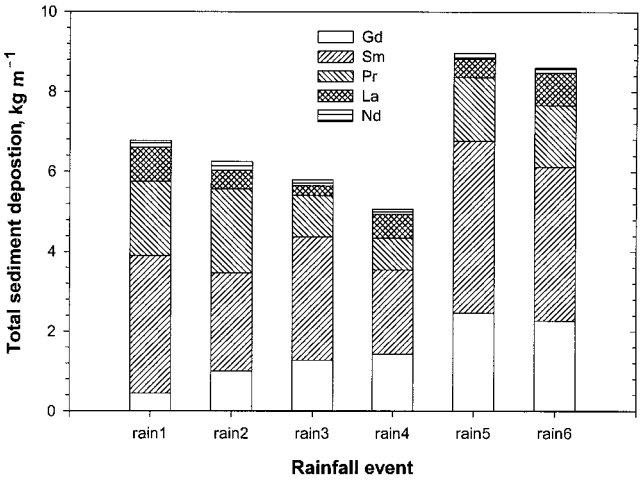

Fig. 8. Total sediment deposition (D^n) per unit plot width from each segment and for six rainfall events.

The largest portion of deposition on the entire slope was from the Sm segment, followed by the Pr and Gd segments (Fig. 8). Depositions from the La and Nd segments were minimal. Interestingly, most of sediment discharge measured at the plot outlet was originally from the Sm and Pr segments (Fig. 5B). Since quasi-steady state conditions existed for much of the time as discussed earlier, a snap shot of a system at or near the end of a rainfall event should adequately reflect the state of the system of any time. Thus, the amounts of deposition following each rain reflected the amounts of steady deposition occurring or existing at any time during that rain. These steady deposition amounts were positively related to amounts of steady sediment discharge. For example, the proportions of deposition from different segments in Rain 3 (Fig. 8) corresponded well to those of steady sediment discharge in Fig 4B. Since most of the measured deposition occurred in interrill areas, such positive relations may suggest that (i) interrill erosion played an important role in supplying sediment to concentrated flow under this experimental condition, and (ii) detachment, transport, deposition, and redetachment occur simultaneously and continuously in interrill areas. The later inference can be better understood if the interrill erosion is viewed as splash and saltation type transport by raindrop impacted sheet flow. This finding indicates that chances for soil particles being delivered to concentrated flow are proportional to the extent of those particles being continuously deposited and dislodged in the interrill areas.

Sediment delivery ratio for each individual rain, calculated with Eq. [8], is given in Table 4. The ratio for the first rain is an exact estimate, while others are lower-bound values. The first rain's sediment delivery ratio was only 0.18, indicating a significant amount of sediment deposition. The delivery ratios increased to >0.40 for all the subsequent rains, showing greater sediment transport efficiency because of progressive development of a concentrated-flow network. This demonstrates that the REE tracing method has the potential to estimate sediment delivery ratios. The erosion equilibrium indices, calculated with Eq. [9], in Table 4 indicate that net deposition predominated in Rains 1 and 5; small net detachment took place in Rains 2, 3, and 6; and most severe net detachment occurred in Rain 4. These results substantiate the earlier conclusion that a quasi-steady state or somewhat balanced detachment-transport-deposition system existed in Rains 2, 3, and 6.

CONCLUSIONS

Five REE oxides were directly mixed with a silt soil in five individual bands on a 4-m uniform slope to trace soil erosion during six simulated rains. Relative errors of REE-derived event sediment discharge decreased steadily from 26% for Rain 1 to 4% for Rain 6, with a mean of 14.5%. The large initial error could be attributed to the nonuniform tracing method, in which only 19% of the plot area was tagged with tracers. If higher accuracy is desired, a whole area tagging method should be used.

The most severe soil erosion occurred in the upper middle slope sections during the six consecutive rains. This finding challenges the wisdom that the most severe erosion takes place in the lower slope sections of a uniform slope. However, this result needs to be tested further at various slopes and slope lengths. Large net deposition took place in Rains 1 and 5 when the rainfall intensity was elevated, and considerable net detachment occurred in Rain 4. However, a somewhat balanced detachment-transport-deposition system existed in Rains 2, 3, and 6. Interestingly, total sediment delivery from each segment was positively related to amounts of total sediment deposition on the entire slope from that segment.

Results suggest that upland soil erosion is a continuous, simultaneous, and interactive detachment, transport, and deposition process that varies in both time and space. The REE tracing technique is capable of generating spatially and temporally distributed data that could provide insights into erosion processes, which

Table 4. Measured sediment discharge (T^n), estimated total deposition after each rain (D^n), net deposition during each rain ($D^n - D^{n-1}$), sediment delivery ratio (ρ^n), and erosion equilibrium index.

Rainfall event	Measured sediment discharge	Estimated total deposition	Net deposition per event	Delivery ratio	Equilibrium index
	g m^{-1}				
1	1530	6771	6771	0.18	0.18
2	4378	6248	−523	0.41	1.14
3	3815	5795	−453	0.40	1.13
4	3527	5068	−727	0.41	1.26
5	7129	8972	3904	0.44	0.65
6	7135	8603	−369	0.45	1.05

would be impossible using traditional erosion measurement methods. A field study is currently underway to assess further its applicability and feasibility at a 0.68-ha watershed. The preliminary results from this study have indicated that this new technique is promising and may provide us a unique means to further our understanding of soil erosion processes and their dynamics along a hill slope profile or in a small watershed.

REFERENCES

Borah, D.K. 1989. Sediment discharge model for small watersheds. Trans. ASAE 32:874–880.

Flanagan, D.C., C. Huang, L.D. Norton, and S.C. Parker. 1995. Laser scanner for erosion plot measurements. Trans. ASAE 38:703–710.

Foster, G.R., and L.D. Meyer. 1972. A closed-form soil erosion equation for upland areas. p. 12.1–12.19. *In* H.W. Shen (ed.) Sedimentation. Colorado State University, Fort Collins, Co.

Hairsine, P.B., and C.W. Rose. 1992. Modeling water erosion due to overland flow using physical principles 2. rill flow. Water Resour. Res. 28:245–250.

Huang, C., and J.M. Bradford. 1990. Portable laser scanner for measuring soil surface roughness. Soil Sci. Soc. Am. J. 54:1402–1406.

Institute of Soil and Water Conservation. 1997. A special publication on application of rare earth elements for soil erosion studies. (In Chinese with English abstract). Res. Soil Water Conserv. 4:2:112.

Jarvis, K.E. 1989. Elemental analysis of the lanthanides. P. 65–92. *In* J.C.G. Bunzli and G.R. Choppin (ed.) Lanthanide Probes in life, chemical and earth sciences. Elsevier Science, Amsterdam, The Netherlands.

Nearing, M.A., G.R. Foster, L.J. Lane, and S.C. Finkner. 1989. A process-based soil erosion model for USDA-water erosion prediction project technology. Trans. ASAE 32:1587–1593.

Nearing, M.A., G. Govers, and L.D. Norton. 1999. Variability in soil erosion data from replicated plots. Soil Sci. Soc. Am. J. 63:1829–1835.

Olmez, I., F.X. Pink, and R.A. Wheatcroft. 1994. New particle-labeling technique for use in biological and physical sediment transport studies. Environ. Sci. Technol. 28:1487–1490.

Plante, A.F., M.J.M. Duke, and W.B. McGill. 1999. A tracer sphere detectable by Neutron Activation for soil aggregation and translocation studies. Soil Sci. Soc. Am. J. 63:1284–1290.

Riebe, B. 1995. Monitoring the translocation of soil particles using a neutron activated tracer. p. 277–297. *In* K.H. Hartge and B.A. Stewart (ed.) Soil structure: Its development and function. CRC Press, Boca Raton, FL.

Ritchie, J.C., and J.R. McHenry. 1990. Application of radioactive fallout Cesium-137 for measuring soil erosion and sediment accumulation rates and patterns: A review. J. Environ. Qual. 19:215–233.

Tian, J.L., P.H. Zhou, and P.L. Liu. 1994. REE tracer method for studies on soil erosion. Int. J. Sediment Res. 9:39–46.

Toth, S.J., and R.B. Alderfer. 1960. A procedure for tagging water-stable soil aggregates with Co-60. Soil Sci. 89:36–37.

Ventura, E., Jr., M.A. Nearing, and L.D. Norton. 2001. Developing a magnetic tracer to study soil erosion. Catena 43:277–291.

Wallbrink, P.J., and A.S. Murray. 1993. Use of fallout radionuclides as indicators of erosion processes. Hydrol. Processes. 7:297–304.

Walling, D.E., and T.A. Quine. 1990. Calibration of Cesium-137 measurements to provide quantitative erosion rate data. Land Degrad. Rehab. 2:161–175

Walling, D.E., and Q. He. 1999. Improved models for estimating soil erosion rates from cesium-137 measurements. J. Environ. Qual. 28:611–622.

Wooldridge, D.D. 1965. Tracing soil particle movement with Fe-59. Soil Sci. Soc. Am. Proc. 29:469–472.

Young, R.A., and R.F. Holt. 1968. Tracing soil movement with fluorescent glass particles. Soil Sci. Soc. Am. Proc. 32:600–602.

Zhang, X.C., J.M. Friedrich, M.A. Nearing, and L.D. Norton. 2001. Potential use of rare earth oxides as tracers for soil erosion and aggregation studies. Soil Sci. Soc. Am. J. 65:1508–1515.

Zhang, X.C., M.A. Nearing, W.P. Miller, L.D. Norton, and L.T. West. 1998. Modeling interrill sediment delivery. Soil Sci. Soc. Am. J. 62:438–444.